Structure and Thermodynamics of Empty Clathrate Hydrates bellow the Freezing Point of H_2O

ORAL

(Energy and Environment)

Fernando J.A.L. Cruz[*] *and José P.B. Mota*

[1] *LAQV@Requimte, Dept. Chemistry, NOVA University Lisbon, 2829-516 Caparica; *fj.cruz@fct.unl.pt.*

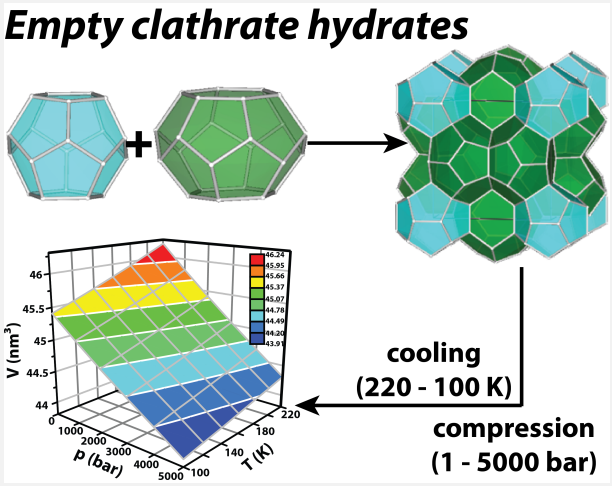

Simulations are employed to probe empty *sI* and *sII* clathrate hydrates, observing that the volumetric response to an applied $p-T$ gradient is accurately described by the Parsafar and Mason equation of state with an accuracy > 99%. Structural deformation induced upon the crystals is monitored and benchmarked against previous neutron diffraction measurements of ice XVI and hexagonal ice at 1 bar. A critical comparison is established with guest occupied lattices (CH_4, CO_2 and C_nH_{2n+2}), revealing that empty *sII* frameworks are slightly more stable to thermal deformation than their *sI* analogues. Of paramount importance for the oil and natural gas industries, heat capacities obtained are identical for the *sI* and *sII* lattices up to 2000 bar and diverge by ~ 7.3 % at 5000 bar. The canonical tetrahedral symmetry of water-bonded networks is analysed in terms of an angular and a distance order parameters, which are observed to decrease (increase) as pressure (temperature) increases (decreases).

Introduction & Methodology. The thermodynamical phase space of the metastable empty clathrate hydrates (CHs) is probed over broad temperature and pressure ranges ($100 \leq T/\mathrm{K} \leq 220$, $1 \leq p/\mathrm{bar} \leq 5000$), using large-scale computer simulations and compared with available experimental data at 1 bar [1, 2]. For that purpose, we employ the fully atomistic and rigid TIP4P-Ice four-charge potential [3] to describe the H_2O lattice of the empty clathrate phases (*sI*, *sII*); this potential was developed to reproduce the experimental melting point of ice *Ih* (272.2 K at 1 bar), and has been successfully employed to study the deformation [1, 2, 4], energetics and decomposition [5, 6], and phase behaviour [7-9] of several CHs. Starting from an initial configuration at the lowest temperature and pressure (100 K, 1 bar), CHs are isothermally pressurised to achieve the desired pressure (1 bar→100 bar→500 bar→1000 bar→2000 bar→5000 bar), and the protocol repeated for the next higher temperature (100 K→120 K→140 K→160 K→180 K→200 K→220 K) starting from the corresponding previous equal pressure run. Calculations are run for at least 50 ns in order to obtain statistically consistent data, and the first 5 ns discarded to account for equilibration. Because data collection takes place every 5 ps, each p–V–T state point is obtained from time-averaging an *ensemble* of 9000 data points. The whole p–V–T surface obtained (*cf.* Graphical Abstract) is interpreted using the universal form of the Parsafar and Mason equation of state [10], always with an accuracy better than 99 %.

Results – Structure. Measurements of unit cell length, a, were conducted during the simulations and are here represented in Figure 1a for the room pressure systems, along with data previously obtained for other guest occupied *sII* CHs. A critical comparison is established in terms of the ratio of molecular diameters between the guest molecule, D_G, and cavity diameter, D_C, allowing the parameter (D_G/D_C) to be used as the rationale for unit cell length increase/contraction when the empty crystals become occupied by guest molecules. Furthermore, the solids' isobaric thermal expansivity, obtained in terms of a parabolic line (Fig. 1b), $\alpha_p = [\partial a/(a \cdot \partial T)]_p$, reveals that the empty CHs exhibit a positive thermal expansion up to a certain temperature threshold, beyond which $[\partial^2 a/(a \cdot \partial T^2)]_p$ becomes negative; the particular temperature at which this phenomenon occurs decreases with applied pressure, and, in the case of the *sII* lattices, starts at 191.5 K@1 bar until finally reaching 161.6 K@5000 bar (Fig.1b).

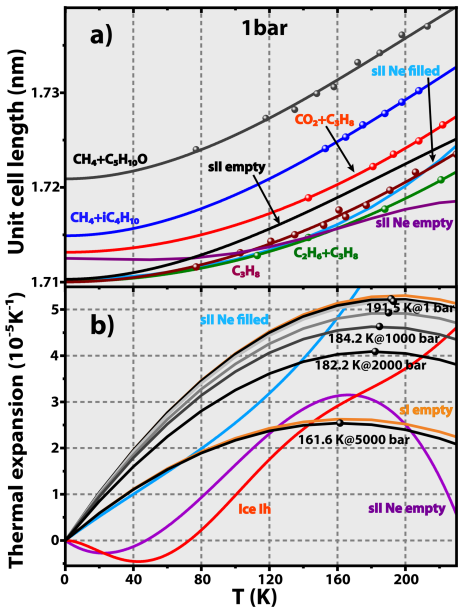

Figure 1. Structural data. ***a***) Temperature dependence of unit cell length at 1 bar for *sII* lattices: symbols correspond to experimental measurements of C_3H_8 (dark red), 18.2 % CO_2 + 81.8% C_3H_8 (light red), 30 % C_2H_6 + 70% C_3H_8 (green), 87.6 % CH_4 + 12.4 % iC_4H_{10} (blue) and 95 % CH_4 + 5 % $C_5H_{10}O$ (dark grey). Results obtained in this work for empty sII clathrates (black), as well as data for Ne-filled (light blue) and Ne-empty (magenta) sII topologies are represented by lines obtained using cubic polynomial fittings. ***b)*** isobaric thermal expansivities, $\alpha_p = (1/a)(\partial a/\partial T)_p$ obtained using molecular simulations and empty *sII* (black) and *sI* clathrates (dark yellow), and previous atmospheric pressure experimental data for hexagonal ice (red) and Ne-filled and Ne-emtpy sII clathrates (light blue, magenta); values represent the several α_p maxima.

The characteristic tetrahedral structure around oxygen atoms was probed using two order parameters, S_g and S_k, in order to monitor the angular and distance contributions to a canonical tetrahedral symmetry, respectively [11]. Time-averaged distributions reveal that the empty frameworks retain tetrahedral integrity throughout the entire *p*–*T* domain, but respond accordingly by slightly distorting the solid lattice. Using Gaussian statistics, it becomes clear that by imposing isothermal conditions whilst increasing pressure, S_g maxima are shifted towards higher values, as a result of the solid contraction and gradual loss of tetrahedral order. For (*p*,*T*) > (2000 bar, 200 K), deformation occurs via a mechanism that involves a dominant contribution from angular alterations. The microscopic structure associated with the solids is probed deeper calculating radial distribution functions (g_r), and, in general, both the g_r(O – O) and g_r(O – H) curves exhibit two maximum intensity peaks, corresponding to the thickness of the first and second order neighbour shells, centered at $r_{(O-O)}$ = (0.27, 0.45) nm and $r_{(O-H)}$ = (0.18, 0.32) nm, revealing that the hydrogen bonds responsible for network integrity are of similar length regardless of the particular (*p*, *T*) conditions. A recent neutron diffraction analysis [12] of an empty *sII* hydrate yielded a mean time-space averaged hydrogen bond distance of 0.275 nm, which compares quantitatively with our own average value of $\bar{r}_{(O-H)} = 0.25$ nm.

Results – Thermodynamics. The isobaric heat capacity is obtained using the classical thermodynamic relation $C_p = (\partial H/\partial T)_p$, where *H* is the solid's molar enthalpy. Figure 2 shows a *quasi*-constant correlation with pressure, at least up to 2000 bar, beyond which C_p becomes a function of the clathrate individual topology. When pressure reaches 5000 bar, the *sII* polymorphs exhibit a C_p that is ~ 7.3 % larger than the corresponding *sI* crystals, suggesting that the larger cages characteristic of *sII*, when subject to hydrostatic pressure, are better suited to accommodate heat propagation through the lattice thus giving rise to a slightly enhanced C_p as compared to the *sI* structure. Data obtained for the empty clathrates and also for hexagonal ice have been successfully correlated using Shomate-like equations, $C_p = \mathrm{A} + Bp + Cp^2 + Dp^3$ [2].

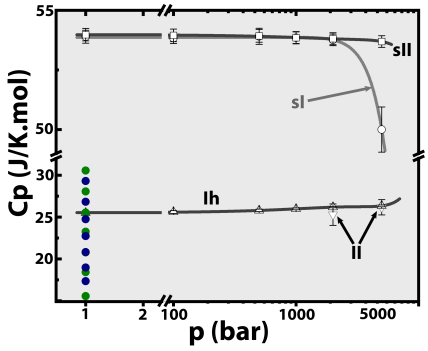

Figure 2. Isobaric heat capacity, C_p. Symbols and error bars correspond to data obtained in the calculations: (□) empty sII clathrates, (○) empty sI clathrates, (△) hexagonal ice Ih and (▽) ice II and experimental results from Handa and Murray for ice (●) and a THF clathrate (●). Lines correspond to cubic polynomials, $C_p = \mathrm{A} + Bp + Cp^2 + Dp^3$. Notice that the C_p scale has been broken in the range 31 – 49.5 J/K·mol.

Handa et al. used a Tian-Calvet heat-flow calorimeter and samples of a tetrahydrofuran CH (THF·16.9H_2O) and H_2O ice, at 85–270 K at room-pressure [13, 14]. Under their experimental conditions, hexagonal ice is the thermodynamically stable form of water, for which the isobaric heat capacity was observed to increase from C_p = 15.5 J/K·mol up to C_p = 30.5 J/K·mol, when temperature climbs from 100 K to 220 K, respectively, giving rise to an average value of $\overline{C_p}$ = 23 J/K·mol, in satisfactory agreement with our own result of C_p = 25.5 J/K·mol. For the THF hydrate samples C_p = 17.4 J/K·mol (100 K) and 29.3 J/K·mol (220 K). Their complete set of calorimetric data for ice *Ih* and THF·16.9H_2O is graphically represented in Figure 2, together with the results obtained in the present work.

Acknowledgements

This work received support from PT national funds (FCT/MCTES, Fundação para a Ciência e Tecnologia and Ministério da Ciência, Tecnologia e Ensino Superior) through projects UIDB/50006/2020 and UIDP/50006/2020. F.J.A.L.C. gratefully acknowledges FCT/MCTES for funding through program DL 57/2016 – Norma Transitória (Ref. 654/2018-24), and also for funding the Advanced Computing Project 2021.09623.CPCA on Cirrus-A:INCD.

References

[1] F.J.A.L. Cruz *et al.*, ACS Earth Space Chem., 3 (2019) 789. [2] F.J.A.L. Cruz, J.P.B. Mota, Phys. Chem. Chem. Phys., 23 (2021) 16033. [3] J.L.F. Abascal *et al.*, J. Chem. Phys., 122 (2005) 234511. [4] S. Takeya *et al.*, J. Phys. Chem. C, 122 (2018) 8134. [5] S. Alavi, R. Ohmura, J. Chem. Phys., 145 (2016) 154708. [6] S.A. Bagherzadeh *et al.*, J. Chem. Phys., 142 (2015) 214701. [7] H. Tanaka *et al.*, J. Chem. Phys., 149 (2018) 074502. [8] D. Jin, B. Coasne, Langmuir, 33 (2017) 11217. [9] V.K. Michalis *et al.*, J. Chem. Phys., 142 (2015) 044501. [10] G. Parsafar, E.A. Mason, Phys. Rev. B, 49 (1994) 3049. [11] P.-L. Chau, A.J. Hardwick, Mol. Phys., 93 (1998) 511. [12] A. Falenty *et al.*, Nature, 516 (2014) 231. [13] Y.P. Handa, Can. J. Chem., 62 (1984) 1659. [14] Y.P. Handa *et al.*, J. Chem. Thermodyn., 16 (1984) 623.